



Research Article

Study on Vibration and Bifurcation of an Aeroengine Rotor System with Elastic Ring Squeeze Film Damper

Guoying Pang ^{1,2}, Shuqian Cao ^{1,2}, Yushu Chen,^{1,2} and Huizheng Chen³

¹Department of Mechanics, Tianjin University, Tianjin 300354, China

²Tianjin Key Laboratory of Nonlinear Dynamics and Control, Tianjin 300354, China

³Institute of Dynamics and Control Science, Shandong Normal University, Jinan 250014, China

Correspondence should be addressed to Shuqian Cao; sqcao@tju.edu.cn

Received 2 June 2021; Revised 15 September 2021; Accepted 28 September 2021; Published 19 October 2021

Academic Editor: Seyed M. Hashemi

Copyright © 2021 Guoying Pang et al. This is an open access article distributed under the Creative Commons Attribution License, which permits unrestricted use, distribution, and reproduction in any medium, provided the original work is properly cited.

To analyze the problem of vibration and bifurcation in the rotor system of the aeroengine with the elastic ring squeeze film damper (ERSFD) and elastic supports, the theoretical equation of the dynamic rotor system is developed in this paper, based on the rotor system, elastic ring squeeze film damper (ERSFD), and three elastic supports. The estimated analytical solution of the oil film force is solved using the short bearing approximation theory and the semi-oil film inference theory in the suspension and the inner and outer boss contact. Considering the oil film stiffness and damping of rolling bearings, the rolling bearing force model is established based on the elasto-hydrodynamic lubrication (EHL) theory. By the average method, the vibration and bifurcation modes are obtained concerning the bearing coefficient and parameters. The range optimization of parameters can be appropriately improved to enhance the dynamic characteristics of the device given different parameters of the hole of oil seepage, the stiffness, the position of elastic supports, and other structural parameters.

1. Introduction

Based on the squeeze film damper (SFD), Russian scholars proposed an elastic ring squeeze film damper (ERSFD). The basic principle is to leave the appropriate clearance between the outer ring of the rolling bearing and bearing support. The elastic ring and the lubricating oil were added to the clearance. The vibration attenuation effect is mediated by the journal vortex extrusion between the inner and outer rings of the lubricating oil as well as the elastic band. The inner and outer surfaces of the elastic ring are machined with many bosses, which are staggered and uniformly distributed. The inner surface boss is matched with the outer ring of the bearing surface, and the outer surface boss is matched with the inner surface of the bearing surface. It can be divided into four situations based on the interaction between the elastic ring, the journal, and the bearing seat: outer bosses contact, inner bosses contact, inner and outer bosses contact, and suspension. Owing to its simple structure, limited occupation space, noticeable vibration reduction, more vital system

stability, and other characteristics, it has been successfully applied to various aeroengines.

The structural style of the rotor system, nonlinear characteristics of the elastic ring squeeze film damper, Reynolds equation solution, experimental design, and simulation have provided plenty of research information. Experiments by Zhu and Feng [1] examined the effect of oil film radial clearance, unbalance value, and centering spring stiffness on the phenomenon of vibration in a rotor-squeeze film damper system. Meng and Xia [2] investigated the action of bifurcation and chaos in the design of a flexible rotor and a nonconcentric squeeze film damper under an excitation response. The critical paths of response to chaos are the periodic bifurcation, quasiperiodic bifurcation, and paroxysmal bifurcation into chaos. There are two main ways for the system to exit chaos: periodic and quasiperiodic bifurcations. Xia et al. [3] obtained some parameter combinations to avoid the phenomenon of vibration jumping by analyzing the response curve of the flexible rotor system and the squeeze film damper. Rezvani and Hahn [4] and Zhao

et al. [5] studied the floating ring squeeze film damper, which effectively improved the bistable phenomenon of the squeeze film damper, and pointed out that the rotor system had obvious bifurcations and quasiperiodic motions above two times the critical speed. Wang et al. [6] used CFD to analyze the deformation influence of ERSFD and introduced the Zwart–Gerber–Belamri model to reveal the adaptive mechanism of the thickness of the oil film. Han et al. [7] calculated the deformation of an elastic ring based on the Kirchhoff hypothesis and numerically simulated the dynamics and response of the rotor system. Wang et al. [8] used a numerical method to improve the fluid-structure coupling calculation model of the ERSFD and built a test bench to test the dynamic characteristic coefficients of the elastic ring and oil film. Furthermore, they proposed that the oil film force of the elastic ring leads to the complex deformation of the elastic ring and affects the contact state of bosses of the elastic ring. Li et al. [9] constructed a rotor system with ERSFD. The characteristics of vibration reduction in each state of the elastic ring were investigated experimentally by adjusting the fit of the pedestals on the elastic ring and the unbalance value of the rotor. Based on the findings, the inner pedestals of the elastic ring should be clearance-fitted according to the ERSFD specification. Xu et al. [10] studied the dynamic characteristics of the elastic ring of the distribution of oil seepage holes and the design of the oil seepage hole position under the optimal damping of the elastic ring. The dynamic characteristics of the damper were significantly influenced by the coordination relationship between the inner and outer bosses of the elastic ring.

In conclusion, most research based on numerical simulation and experimental analysis of the ERSFD or SFD rotor system focused on the theoretical solution of the dynamical model. The theoretical derivation process of the affecting efficiency of related factors has not been studied, especially the elastic ring, journal, and bearing support during various contacts. The research object in this paper study is the vibration and bifurcation of an aeroengine rotor system with ERSFD when the elastic ring is in the suspension and the inner and outer boss contact between the journal and bearing seat. The ERSFD model was estimated using geometric relationships. The approximate analytical solution of the oil film force was obtained using the short bearing approximation theory and semi-oil film inference theory. The moderate equations by the average method examine the effect of parameters on the amplitude frequency characteristics and the system's optimum parameter range.

2. The Structure of ERSFD Rotor System

The aeroengine rotor test bench was simplified as a rigid rotor with elastic supports, as shown in Figure 1. On the left-hand side, there are elastic supports 1 and 2, and their bearing stiffness are k_1 and k_2 , respectively. Elastic support 2 is parallel to the ERSFD, which is l_1 away from elastic support 1. Elastic support 3 is installed on the right side, and its bearing stiffness is k_3 .

The basic structure of the elastic supports is as follows: The inner ring of the bearing is fixed on the rotor and rotates

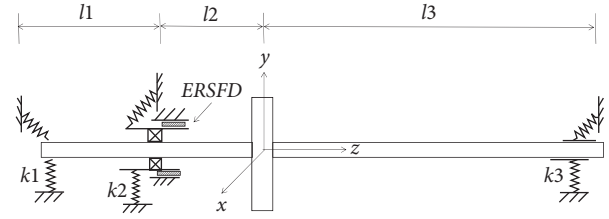


FIGURE 1: Schematic diagram of the rotor system with elastic ring squeeze film damper.

with the rotor. The outer ring is fixed to the inner ring of the cage and held motionless. The ball or roller is evenly distributed around the inner ring. There is only pure rolling between the rollers and the inner and outer rings, with no sliding. Contact is an ideal contact, and the contact stress conforms to the Hertz contact theory. The structural order of the supporting structure of the ERSFD from inside to outside is as follows: rotor, inner ring of bearing, ball (or roller), outer ring of bearing, squirrel cage, inner oil film, elastic ring, outer oil film, engine casing. To analyze the dynamic characteristics of the rotor system, the oil film force of the ERSFD and the bearing force of the rolling bearings are analyzed in detail.

2.1. The Model of the Oil Film Force of the ERSFD. According to the design of Russian scholars, the theory of hydrodynamic lubrication can calculate the oil film force of the ERSFD, and the elastic ring passes on the hydrodynamic pressure. They analyzed the motion process of the elastic ring from the perspective of simulations and experiments [8–10]. In this study, a theoretical model is established for analysis: (1) The pressure model of the inner layer of the oil film is established under the suspension and the inner and outer bosses contact. (2) Using the short bearing theory, the oil film forces of these structures are obtained. (3) The approximate analytical solution of the oil film force is consistent with the actual situation when the semi-Sommerfeld theory boundary theory is assumed. The expression is also given in the rectangular coordinate system.

The following simplified assumptions are made to analyze the flow field of ERSFD. (1) Film hypothesis: the oil film is considered so thin that the velocity gradient in the thickness direction is more important than the velocity gradient in any other direction. (2) Fluid is an incompressible flow, and the oil film flow is a laminar flow with no eddy current and turbulence, in line with Newton's law of viscosity. (3) The effects of temperature and fluid volume force are not considered. (4) Ignoring the journal curvature effect, the journal moves in a circle [11].

Considering that the elastic ring with bosses and oil seepage holes is subjected to extrusion motion from the axial direction and diameter, the movement process is from the suspension to the inner bosses contact. Owing to the eccentricity depicted in Figure 2, e_1 and e_2 are the eccentricity of the journal O_j and the elastic ring O_f with the bearing seat O_b . e_3 is the relative eccentricity of the journal O_j and the elastic ring O_f . μ is the viscosity of the oil film. Ω_1 is the

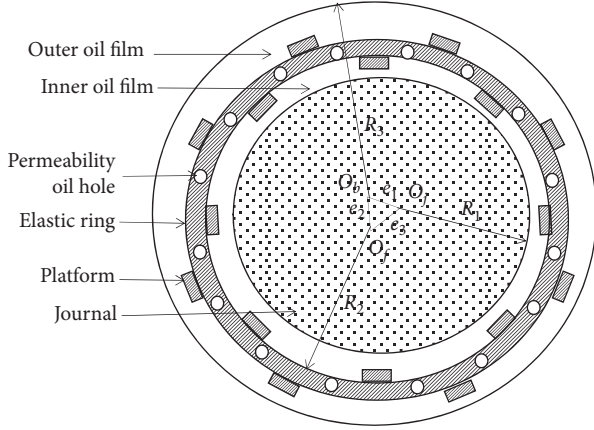


FIGURE 2: Structure diagram of elastic ring squeeze film damper.

precession speed of the journal. Ω_2 is the precession speed of the elastic ring.

In the suspension, the inner and outer bosses of the elastic ring do not contact the outer surface of the bearing and the inner surface of the bearing seat in the precession process of the elastic ring and the journal. Moreover, the oil film of the elastic ring is divided into the inner and outer layers of the oil film. The center of the elastic ring, the center of the journal, and the center of the bearing seat are eccentric.

According to the relationship of geometry [11–13] and the transient Reynolds equation of ERSFD, the maximum oil film clearance is measured and analyzed separately. θ_1 and θ_2 are the included angles from the maximum oil film thickness of the inner and the outer oil films, respectively. The equations for the oil film pressure were derived.

- (1) The equation of the inner oil film pressure of the suspension is

$$\frac{1}{R_1^2} \frac{\partial}{\partial \theta_1} \left(h_1^3 \frac{\partial p_1}{\partial \theta_1} \right) + \frac{\partial}{\partial Z} \left(h_1^3 \frac{\partial p_1}{\partial Z} \right) = 12\mu e_{11} \sin \theta_1 + 12\mu e_{12} \cos \theta_1 + 12\mu v_d. \quad (1)$$

- (2) The equation of the outer oil film pressure of the suspension is

$$\frac{1}{(R_2 + h_{01} + h_{00}\delta_0)^2} \frac{\partial}{\partial \theta_2} \left(h_2^3 \frac{\partial p_2}{\partial \theta_2} \right) + \frac{\partial}{\partial Z} \left(h_2^3 \frac{\partial p_2}{\partial Z} \right) = 12\mu e_{21} \sin \theta_2 + 12\mu e_{22} \cos \theta_2 + 12\mu v_d, \quad (2)$$

where h_{00} is the height of the inner and outer bosses. h_{01} is the thickness of the elastic ring. When the height of the boss is considered, the indicative function is $\delta_0 = 1$; otherwise, $\delta_0 = 0$. v_d is the flow rate of the oil seepage holes. The clearance of the inner oil film is $c_1 = R_2 - h_{00}\delta_0 - R_1$. The thickness of the inner oil film is $h_1 = c_1 + e_3 \cos \theta$. $c_2 = R_3 - (R_2 + h_{01} + h_{00}\delta_0)$ is the clearance of the outer oil

film. $h_2 = c_2 + e_2 \cos \theta_2$ is the thickness of the outer oil film. $e_{21} = e_2\Omega$. $e_{22} = \dot{e}_2$.

$$\begin{aligned} e_{11} &= \Omega_{01} \frac{e_1^2 + e_3^2 - e_2^2}{2e_3} - \frac{\dot{e}_1}{e_1} \frac{\sqrt{4e_1^2 e_3^2 - (e_1^2 + e_3^2 - e_2^2)^2}}{2e_3} \\ &+ \Omega_{02} \frac{e_2^2 + e_3^2 - e_1^2}{2e_3} + \frac{\dot{e}_2}{e_2} \frac{\sqrt{4e_2^2 e_3^2 - (e_2^2 + e_3^2 - e_1^2)^2}}{2e_3}, \\ e_{12} &= \Omega_{01} \frac{\sqrt{4e_1^2 e_3^2 - (e_1^2 + e_3^2 - e_2^2)^2}}{2e_3} + \frac{\dot{e}_1}{e_1} \frac{e_1^2 + e_3^2 - e_2^2}{2e_3} \\ &- \Omega_{02} \frac{\sqrt{4e_2^2 e_3^2 - (e_2^2 + e_3^2 - e_1^2)^2}}{2e_3} + \frac{\dot{e}_2}{e_2} \frac{e_2^2 + e_3^2 - e_1^2}{2e_3}. \end{aligned} \quad (3)$$

The inner and outer bosses contact is that the inner bosses contact the outer ring of the bearing, and the outer bosses contact the inner surface of the bearing seat. The oil film is divided into inner and outer oil cavities by an elastic ring. The oil film and the elastic ring are compressed by the precession process of the shaft journal to promote oil flow between the oil holes. The extruded elastic ring is equivalent to a fixed inside because of the contact between the inner and outer bosses. Thus, the eccentricity of the elastic ring and the center of the bearing seat are ignored, and only the eccentricity between the elastic ring and the journal exists. θ_3 and θ_4 are the included angles from the maximum thickness of the inner and the outer oil films, respectively. According to the relationship of geometry, the equation of the oil film pressure is derived.

- (3) The equation of the inner oil film pressure of the inner and outer bosses contact is

$$\frac{1}{R_1^2} \frac{\partial}{\partial \theta_3} \left(h_3^3 \frac{\partial p_3}{\partial \theta_3} \right) + \frac{\partial}{\partial Z} \left(h_3^3 \frac{\partial p_3}{\partial Z} \right) = 12\mu e_{31} \Omega \sin \theta_3 + 12\mu e_{32} \cos \theta_3 + 12\mu v_d. \quad (4)$$

- (4) The equation of the outer oil film pressure of the inner and outer bosses contact is

$$\frac{1}{(R_2 + h_{01} + h_{00}\delta_0)^2} \frac{\partial}{\partial \theta_4} \left(h_4^3 \frac{\partial p_4}{\partial \theta_4} \right) + \frac{\partial}{\partial Z} \left(h_4^3 \frac{\partial p_4}{\partial Z} \right) = 12\mu v_d, \quad (5)$$

where the clearance of the inner oil film is $c_3 = R_2 - h_{00}\delta_0 - R_1$. $h_3 = c_3 + e_2 \cos \theta_3$ is the thickness of the inner oil film. $c_4 = h_{00}$ is the clearance of the outer oil film. $h_4 = R_3 - R_2 - h_{01} - h_{00}\delta_0$ is the thickness of the outer oil film. $e_{31} = e_2\Omega$. $e_{32} = \dot{e}_2$. $e_{41} = 0$. $e_{42} = 0$.

The above equations describe the inner and outer layers of the oil film force models of the elastic ring within the suspension and inner and outer bosses contact. Based on the relationships between the two types of combination models and the selection and adjustment of its related parameters, the condition model of the outer bosses contact (the inner oil film pressure model of the suspension and the outer oil film pressure model of the inner and outer bosses contact) and the condition model of the inner bosses contact (the outer oil film pressure model of the suspension and the inner oil film pressure model of the inner and outer bosses contact) are described. Therefore, the Russian scholars' proposed mathematical model of four contact situations of the ERSFD is improved in the construction.

In addition, static eccentricity exists in the installation process of the elastic ring and the journal. Dynamic eccentricity exists between the elastic ring, journal, and bearing seat owing to the precession extrusion process of the journal. The influence of three eccentricities (e_1 , e_2 , and e_3) is considered in this study, which is consistent with reality. If only the eccentricity of the journal and the elastic ring are considered, these models are simplified to their models [10, 11, 13]. Furthermore, the thickness of the elastic ring and the height of the bosses were considered. When different structural parameters are selected, the above four models can be converted into structural models of SFD, PSFD, and FSFD.

The journal structure, elastic ring, and inner oil film between them are mainly analyzed in this study. The short bearing theory solves the inner oil film forces of the suspension and the contact between the inner and outer bosses. When there are sealing devices at both ends of the damper, the boundary condition is considered as

$$\begin{aligned} Z &= -\frac{L}{2}, \\ p &= p_1, \\ Z &= \frac{L}{2}, \\ p &= p_2. \end{aligned} \quad (6)$$

According to the short bearing theory, the radial and circumferential forces of oil film are, respectively,

$$\begin{aligned} F_r &= \frac{1}{12c^3} RL^3 \left[12\mu e_1^* I_3^{11} \Big|_{\theta_1}^{\theta_2} + 12\mu e_2^* I_3^{02} \Big|_{\theta_1}^{\theta_2} + 12\mu \nu_d I_3^{01} \Big|_{\theta_1}^{\theta_2} \right] \\ &\quad - \frac{1}{2} R (p_1 + p_2) L \sin \theta \Big|_{\theta_1}^{\theta_2}, \\ F_t &= \frac{1}{12c^3} RL^3 \left[12\mu e_1^* I_3^{20} \Big|_{\theta_1}^{\theta_2} + 12\mu e_2^* I_3^{11} \Big|_{\theta_1}^{\theta_2} + 12\mu \nu_d I_3^{10} \Big|_{\theta_1}^{\theta_2} \right] \\ &\quad + \frac{1}{2} R (p_1 + p_2) L \cos \theta \Big|_{\theta_1}^{\theta_2}, \end{aligned} \quad (7)$$

where $e_1^* = (e_{11}, e_{21})^T$, $e_2^* = (e_{12}, e_{22})^T$, $I_3^{lm} = \int_{\theta_1}^{\theta_2} (\sin^l \theta \cos^m \theta / (1 + \varepsilon \cos \theta)^3) d\theta$, θ_1 is the starting point of the

positive-force zone of the oil film, and θ_2 is the endpoint of the positive-force zone of the oil film.

The eccentricity is

$$\begin{aligned} \varepsilon &= (\varepsilon_1, \varepsilon_2)^T \\ &= \left(\frac{e_3}{c_1}, \frac{e_2}{c_2} \right)^T \\ &= \left(\frac{e_3}{R_2 - h_{00} \delta_0 - R_1}, \frac{e_2}{h_{00}} \right)^T. \end{aligned} \quad (8)$$

The oil clearance is

$$\begin{aligned} c &= (c_1, c_2) \\ &= (R_2 - h_{00} \delta_0 - R_1, h_{00}). \end{aligned} \quad (9)$$

These studies focused on the suspension and inner and outer bosses contact of the elastic ring. The oil clearance from c_1 to c_2 describes the process from the suspension to the inner and outer bosses contact. Although the changing process has been verified experimentally [9], a mathematical model is established and analyzed theoretically and in depth. According to further analysis, the elastic ring is often fixed by the pin in a particular engine structure to prevent instability. The elastic ring is squeezed by the journal and the oil film and moves in a synchronous circle with the journal.

Assuming that $e_1 = e_2 = e_3 = e$, $e_{11} = e_{21} = e\omega$, $\Omega_{01} = \Omega_{02} = \omega$, $e_{12} = e_{22} = \dot{e}$, combined with the boundary condition of the semi-Sommerfeld theory $\theta_1 = \pi$ and $\theta_2 = 2\pi$, we obtain

$$F_r = \mu R_1 L^3 \left[\omega \frac{2e^2}{(c^2 - e^2)^2} + \pi \dot{e} \frac{(c^2 + 2e^2)}{2(c^2 - e^2)^{5/2}} - 2\pi \nu_d \frac{e}{(c^2 - e^2)^{5/2}} \right], \quad (10)$$

$$F_t = \mu R_1 L^3 \left[\frac{\pi \omega e}{2(c^2 - e^2)^{3/2}} + \dot{e} \frac{2e}{(c^2 - e^2)^2} - \nu_d \frac{2}{(c^2 - e^2)} \right]. \quad (11)$$

The Cartesian coordinate system is changed to

$$\begin{cases} F_x = F_r \frac{x_1}{e} - F_t \frac{y_1}{e}, \\ F_y = F_r \frac{y_1}{e} + F_t \frac{x_1}{e}. \end{cases} \quad (12)$$

Then, $e = \sqrt{x_1^2 + y_1^2}$ is the radial displacement of the journal.

Depending on the different values, combined with equations (10)–(12), the oil film forces of the radial and circumferential are expressions of the oil film force under the state of radial and circumferential in semi-oil film cases and the rectangular coordinate system, when the elastic ring is in the suspension and the inner and outer bosses contact.

Compared with other studies, this model includes the thickness of the elastic ring, height of the bosses, oil

clearance, oil seepage hole, and pressure at both ends, which is more consistent with actual working conditions.

Furthermore, the approximate analytical solutions of the four types of oil film forces can be obtained theoretically using different combinations of oil film forces, which provides a theoretical basis for analyzing complex contact cases of ERSFD.

2.2. The Model of the Bearing Force of the Rolling Bearing. Considering the oil film stiffness and damping of rolling bearings in elastic supports 1, 2, and 3, the elastohydrodynamic lubrication (EHL) model of the shaft bearing is established in this section [14]. It is assumed that the contact zone structure of the lubricant inlet space, Hertz contact space, and lubricant outlet space can be simplified as a spring and viscous damping structure. Ignoring the oil film damping in the Hertz contact space, and the oil film stiffness and damping in the inlet space, the total contact stiffness of the bearings can be connected by the Hertz contact stiffness in the Hertz contact space and the oil film stiffness in series, and then in parallel with the oil film stiffness in the lubricant inlet space. The total damping is the viscous damping of the oil film in the inlet space [15], as shown in Figure 3(b).

In Figure 3(a), the center of the inner and outer rings of the bearing is O . The number of rolling bodies is N_b . The radius of the inner ring of the rolling bearing is R_{bi} . The radius of the outer ring of the rolling bearing is R_{bo} . The angular velocity of the inner ring of the bearing is $\omega_{rotor} = \Omega$. The dotted line indicates the cage of the rolling bearing. The rotating speed of the cage is $\omega_{cage} = \omega_{rotor} (R_{bi}/R_i + R_{bo})$.

The stiffness and damping of the rolling body in contact with the inner and outer raceways are regarded as the series

relation. The total stiffness and damping can be obtained using a complex stiffness equation. They satisfy the following relationship:

$$\begin{cases} k_j = \frac{k_{s1}k_{s2}}{k_i + k_h}, \\ c_j = \frac{c_{s1}c_{s2}}{c_{s1} + c_{s2}}, \end{cases} \quad (13)$$

where the oil film extrusion stiffness between the rolling body and inner ring is k_i . The Hertz contact stiffness between the rolling body and the inner ring is k_{hi} . The oil film extrusion stiffness between the rolling body and the outer ring is k_o . k_{ho} is the Hertz contact stiffness between the rolling body and the outer ring. k_{ei} and c_{ei} are the dynamic pressure stiffness and damping of the oil film inlet space between the rolling body and inner ring, respectively. k_{e0} and c_{e0} are the dynamic pressure stiffness and damping of the oil film inlet space between the rolling body and outer ring, respectively.

The total stiffness between the rolling body and inner ring is $k_{s1} = (k_i k_{hi} / k_i + k_h) + k_{ei}$, and the total damping is $c_{s1} = c_{ei}$. $k_{s2} = (k_o k_h / k_o + k_h) + k_{e0}$ is the total stiffness between the rolling body and the outer ring, and its total damping is $c_{s2} = c_{e0}$.

The relevant stiffness calculation formula and value can be found in [16, 17]. Because the Hertz contact stiffness ($N/m^{1.5}$) is inconsistent with the oil film stiffness (N/m) units, a coordinate transformation is required.

After considering the EHL, the contact stiffness of the rolling bearing is changed and the damping is considered; the rolling bearing force model of the EHL is

$$F_{bx} = \begin{pmatrix} \sum_{j=1}^{N_b} k_j [(x_j - x_0) \cos \theta_j + (y_j - y_0) \sin \theta_j - \delta_0^*]_+^\alpha \\ \sum_{j=1}^{N_b} c_j [(\dot{x}_j - \dot{x}_0) \cos \theta_j + (\dot{y}_j - \dot{y}_0) \sin \theta_j]_+ \end{pmatrix}^T \begin{pmatrix} \cos \theta_j \\ \sin \theta_j \end{pmatrix}, \quad (14a)$$

$$F_{by} = \begin{pmatrix} \sum_{j=1}^{N_b} k_j [(x_j - x_0) \cos \theta_j + (y_j - y_0) \sin \theta_j - \delta_0^*]_+^\alpha \\ \sum_{j=1}^{N_b} c_j [(\dot{x}_j - \dot{x}_0) \cos \theta_j + (\dot{y}_j - \dot{y}_0) \sin \theta_j]_+ \end{pmatrix}^T \begin{pmatrix} \sin \theta_j \\ \cos \theta_j \end{pmatrix}, \quad (14b)$$

where x_j , x_0 , y_j , and y_0 represent the horizontal and vertical displacement components of the inner and outer rings of the bearing, respectively. $+$ indicates that the value in brackets is nonnegative. When the value in brackets is less than 0, it is calculated as 0. The initial displacement δ_0^* is related to the static eccentric position of the rotor system.

$\alpha = (10/9)$ represents roller bearing. $\alpha = (3/2)$ represents ball bearing. $\theta_j = (2\pi/N_b)(j-1) + \omega_{cage} \times t$ is the azimuth of the first roller.

Based on the geometric structure and force analysis, the model and expression of oil film force and bearing force of the ERSFD rotor system are established, and

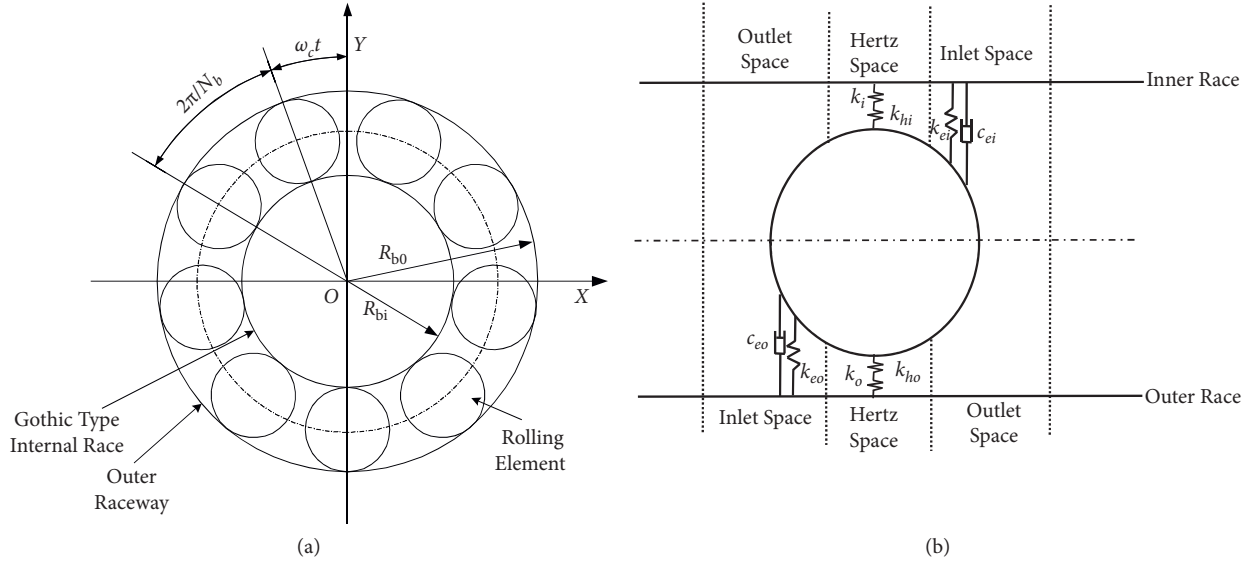


FIGURE 3: EHL (elastohydrodynamic lubrication) model of shaft bearing. (a) Geometric construction. (b) Contact mechanics model.

further analysis shows that the rotor rotates and proceeds during the movement of the rotor. The cage precesses and extrudes the oil film. The oil film force varies over time. In the rotating process of the rolling bearing cages, each roller passes through the lowest point of the inner ring in turn, and the contact stiffness of the roller and rotor is also the periodic variable stiffness [14, 18].

Therefore, in the rotor dynamics equation, there are several expressions for force. (1) A simplified expression of the force is adopted. (2) The partial derivative of its approximate analytical solution with respect to displacement is adopted in the form of equivalent stiffness and damping. (3) The form of the fitting test data and numerical calculations (finite element method, Ansys software, etc.) can also be adopted. These methods can also be used to evaluate the equivalent stiffness and damping, such as the ratio calculation method, least square method, and finite element model. Shi et al. [9, 19] show that the least square method reflects the linear relationship between load of rings and corresponding deformation better, and the calculation results have better accuracy and stability.

Here, in order to carry out subsequent analysis and research, the oil film force is analyzed using the short bearing theory in the form of an approximate analytical solution obtained by formulas (10) and (11). The stiffness and damping of the bearing force are analyzed using the adaptive method and polynomial fitting method to obtain specific data of formulas (13), (14a), and (14b) based on the relevant results [18, 19]. The stiffness k_{mc} of the squirrel cage can be found in literature [20–22]. Therefore, the overall stiffness and damping of the supporting structure can be obtained through a series and parallel structures.

3. Theoretical Analysis of ERSFD Rotor System

By analyzing the kinetic energy, elastic potential energy, dissipated energy, and excitation force generated by the unbalanced mass, the differential equation of the rotor system vibration established by the Lagrange method is as follows:

$$\begin{cases}
 m\ddot{x} + (c_1 + c_2 + c_3)\dot{x} + [c_1(l_1 + l_2) + c_2l_2 - c_3l_3]\dot{\theta}_y + (k_1 + k_2 + k_3)x \\
 + [k_1(l_1 + l_2) + k_2l_2 - k_3l_3]\theta_y + F_x = \delta\omega^2 \cos(\omega t), \\
 m\ddot{y} + (c_1 + c_2 + c_3)\dot{y} - [c_1(l_1 + l_2) + c_2l_2 - c_3l_3]\dot{\theta}_x + (k_1 + k_2 + k_3)y \\
 - [k_1(l_1 + l_2) + k_2l_2 - k_3l_3]\theta_x + F_y = \delta\omega^2 \sin(\omega t), \\
 J_d\ddot{\theta}_x + J_p\omega\dot{\theta}_y - [c_1(l_1 + l_2) + c_2l_2 - c_3l_3]\dot{y} + [c_1(l_1 + l_2)^2 + c_2l_2^2 + c_3l_3^2]\dot{\theta}_x \\
 - [k_1(l_1 + l_2) + k_2l_2 - k_3l_3]y + [k_1(l_1 + l_2)^2 + k_2l_2^2 + k_3l_3^2]\theta_x - F_y l_2 = 0, \\
 J_d\ddot{\theta}_y - J_p\omega\dot{\theta}_x + [c_1(l_1 + l_2) + c_2l_2 - c_3l_3]\dot{x} + [c_1(l_1 + l_2)^2 + c_2l_2^2 + c_3l_3^2]\dot{\theta}_y \\
 + [k_1(l_1 + l_2) + k_2l_2 - k_3l_3]x + [k_1(l_1 + l_2)^2 + k_2l_2^2 + k_3l_3^2]\theta_y + F_x l_2 = 0,
 \end{cases} \quad (15)$$

where k_i is the bearing stiffness of the elastic support i . c_i is the bearing damping of elastic support i , $i = 1, 2, 3$. k_i and c_i are obtained between the stiffness and damping of the squirrel cage and the rolling bearings through series and parallel structures. l_1 is the distance between elastic support 1 and elastic support 2. l_2 is the distance between the disk center and elastic support 2. l_3 is the distance between the disk center and elastic support 3. m is the equivalent mass of the center disk-shaft structure. δ is the unbalance value. J_d

and J_p are the equivalent equatorial inertia and equivalent polar inertia, respectively. F_x is the oil film force in the direction x . F_y is the oil film force in the direction y . x and y are displacements of the node of the equivalent mass in the plane xoy .

Assuming that $q_1 = x + iy$, $\dot{q}_1 = \dot{x} + i\dot{y}$, $\ddot{q}_1 = \ddot{x} + i\ddot{y}$, $q_2 = \theta_y l_2 - i\theta_x l_2$, $\dot{q}_2 = \dot{\theta}_y l_2 - i\dot{\theta}_x l_2$, $\tau = \omega_0 t$, $\ddot{q}_2 = \ddot{\theta}_y l_2 - i\ddot{\theta}_x l_2$, (15) is transformed into

$$\begin{aligned} m(\ddot{x} + i\ddot{y}) + (c_1 + c_2 + c_3)(\dot{x} + i\dot{y}) + (k_1 + k_2 + k_3)(x + iy) + [c_1(l_1 + l_2) + c_2 l_2 - c_3 l_3](\dot{\theta}_y - i\dot{\theta}_x) \\ + [k_1(l_1 + l_2) + k_2 l_2 - k_3 l_3](\theta_y - i\theta_x) + F_x + iF_y = \delta\omega^2 \cos(\omega t) + i\delta\omega^2 \sin(\omega t) \\ J_d(\ddot{\theta}_y - i\ddot{\theta}_x) + [-iJ_p\omega + c_1(l_1 + l_2)^2 + c_2 l_2^2 + c_3 l_3^2](\dot{\theta}_y - i\dot{\theta}_x) + [k_1(l_1 + l_2)^2 + k_2 l_2^2 + k_3 l_3^2](\theta_y - i\theta_x) \\ + [c_1(l_1 + l_2) + c_2 l_2 - c_3 l_3](\dot{x} + i\dot{y}) + [k_1(l_1 + l_2) + k_2 l_2 - k_3 l_3](x + iy) + F_x l_2 + iF_y l_2 = 0. \end{aligned} \quad (16)$$

For the convenience of subsequent discussion, it is abbreviated as

$$M\ddot{q} + (-i\omega G + C)\dot{q} + Kq + F_c = F_u, \quad (17)$$

where

$$M = \begin{pmatrix} m & 0 \\ 0 & J_d \end{pmatrix}, \quad G = \begin{pmatrix} 0 & 0 \\ 0 & J_p \end{pmatrix}, \quad C = \begin{pmatrix} c_1 + c_2 + c_3 & c_1(l_1 + l_2) + c_2 l_2 - c_3 l_3 \\ c_1(l_1 + l_2) + c_2 l_2 - c_3 l_3 & c_1(l_1 + l_2)^2 + c_2 l_2^2 + c_3 l_3^2 \end{pmatrix}.$$

$$K = \begin{pmatrix} k_1 + k_2 + k_3 & k_1(l_1 + l_2) + k_2 l_2 - k_3 l_3 \\ k_1(l_1 + l_2) + k_2 l_2 - k_3 l_3 & k_1(l_1 + l_2)^2 + k_2 l_2^2 + k_3 l_3^2 \end{pmatrix},$$

$$F_c = (F_x + iF_y) \begin{pmatrix} 1 \\ l_2 \end{pmatrix},$$

$$F_u = \delta\omega^2 e^{i\omega\tau} \begin{pmatrix} 1 \\ 0 \end{pmatrix},$$

$$\begin{aligned} q &= \begin{pmatrix} q_1 \\ q_2 \end{pmatrix} \\ &= \begin{pmatrix} x + iy \\ \theta_y l_2 - i\theta_x l_2 \end{pmatrix}. \end{aligned} \quad (18)$$

The average method was used to analyze the vibration and bifurcation of a rotor system equipped with two elastic supports and an SFD [23]. On this basis, the theoretical mathematical model of the ERSFD and three elastic supports is established by adding the structure of the test bench in this study. From the theoretical point of view, nondimensional integrated unbalance value, nondimensional bearing parameter, stiffness, installation location of the elastic support, ERSFD movement state, oil seepage hole flow, and other related structures are further analyzed deeply for the influence of the vibration. The dimensionless equation is used to analyze the rotor dynamics model theoretically, and (17) is transformed into

$$\begin{cases} m\ddot{q}_1 + (c_1 + c_2 + c_3)\dot{q}_1 + (k_1 + k_2 + k_3)q_1 + [c_1(l_1 + l_2) + c_2 l_2 - c_3 l_3]\dot{q}_2 \\ + [k_1(l_1 + l_2) + k_2 l_2 - k_3 l_3]q_2 + F_x + iF_y = \delta\omega^2 (\cos \omega t + i \sin \omega t), \\ J_d\ddot{q}_2 + [-iJ_p\omega + c_1(l_1 + l_2)^2 + c_2 l_2^2 + c_3 l_3^2]\dot{q}_2 + [k_1(l_1 + l_2)^2 + k_2 l_2^2 + k_3 l_3^2]q_2 \\ + [c_1(l_1 + l_2) + c_2 l_2 - c_3 l_3]\dot{q}_1 + [k_1(l_1 + l_2) + k_2 l_2 - k_3 l_3]q_1 + (F_x + iF_y)l_2 = 0. \end{cases} \quad (19)$$

Select $Q_1 = (q_1/\omega_0 c)$, $Q_2 = (q_2/\omega_0 c)$, $\dot{Q}_1 = (\dot{q}_1/\omega_0 c)$, $\dot{Q}_2 = (\dot{q}_2/\omega_0 c)$, $\ddot{Q}_1 = (\ddot{q}_1/\omega_0 c)$, $\ddot{Q}_2 = (\ddot{q}_2/\omega_0 c)$; the above equation is converted to

$$\left\{ \begin{aligned} & \ddot{Q}_1 + \frac{k_1 + k_2 + k_3}{m\omega_0^2} Q_1 + \frac{k_1(l_1 + l_2) + k_2l_2 - k_3l_3}{m\omega_0^2 l_2} Q_2 \\ & = \frac{\delta}{mc} \frac{\omega^2}{\omega_0^2} (\cos \omega t + i \sin \omega t) - \frac{c_1 + c_2 + c_3}{m\omega_0^2} \dot{Q}_1 - \frac{c_1(l_1 + l_2) + c_2l_2 - c_3l_3}{m\omega_0^2 l_2} \dot{Q}_2 - \frac{1}{m\omega_0^2 c} (F_x + iF_y), \\ & \ddot{Q}_2 + \frac{l_2[k_1(l_1 + l_2) + k_2l_2 - k_3l_3]}{\omega_0^2 J_d} Q_1 + \frac{k_1(l_1 + l_2)^2 + k_2l_2^2 + k_3l_3^2}{\omega_0^2 J_d} Q_2 - i \frac{\omega}{\omega_0} \frac{J_p}{J_d} \dot{Q}_2 \\ & = -\frac{c_1(l_1 + l_2)^2 + c_2l_2^2 + c_3l_3^2}{J_d \omega_0^2} \dot{Q}_2 - \frac{l_2[c_1(l_1 + l_2) + c_2l_2 - c_3l_3]}{J_d \omega_0^2} \dot{Q}_1 - \frac{l_2^2}{J_d \omega_0^2 c} (F_x + iF_y). \end{aligned} \right. \quad (20)$$

Namely,

$$\begin{cases} \ddot{Q}_1 + Q_1 + \kappa Q_2 = F_1 + F_{c1} + F_{d1}, \\ \ddot{Q}_2 + \alpha_1 Q_1 + \alpha_2 Q_2 - i\Omega \eta \dot{Q}_2 = F_{c2} + F_{d2}, \end{cases} \quad (21)$$

where $F_c = (F_x + iF_y) \begin{pmatrix} 1 \\ l_2 \end{pmatrix}$, $F_u = \delta \omega^2 e^{i\omega\tau} \begin{pmatrix} 1 \\ 0 \end{pmatrix}$, $q = \begin{pmatrix} q_1 \\ q_2 \end{pmatrix} = \begin{pmatrix} x + iy \\ \theta_y - i\theta_x \end{pmatrix}$, $\tau = \omega_0 t$, $q_1 = x + iy$, $\dot{q}_1 = \dot{x} + i\dot{y}$, $\ddot{q}_1 = \ddot{x} + i\ddot{y}$, $q_2 = \theta_y l_2 - i\theta_x l_2$, $\dot{q}_2 = \dot{\theta}_y l_2 - i\dot{\theta}_x l_2$, $\ddot{q}_2 = \ddot{\theta}_y l_2 - i\ddot{\theta}_x l_2$, $Q_1 = (q_1/\omega_0 c)$, $Q_2 = (q_2/\omega_0 c)$, $\dot{Q}_1 = (\dot{q}_1/\omega_0 c)$, $\dot{Q}_2 = (\dot{q}_2/\omega_0 c)$, $\ddot{Q}_1 = (\ddot{q}_1/\omega_0 c)$, $\ddot{Q}_2 = (\ddot{q}_2/\omega_0 c)$, $\omega_0^2 = (k_1 + k_2 + k_3/m)$, $\kappa = (k_1(l_1 + l_2) + k_2l_2 - k_3l_3/m\omega_0^2 l_2)$, $\Omega = (\omega/\omega_0)$, $U = (\delta/mc)$, $\zeta_1 = (c_1 + c_2 + c_3/m\omega_0^2)$, $\zeta_2 = (c_1(l_1 + l_2) + c_2l_2 - c_3l_3/m\omega_0^2 l_2)$, $\xi_1 = (l_2[c_1(l_1 + l_2) + c_2l_2 - c_3l_3]/J_d \omega_0^2)$, $\eta = (J_p/J_d)$, $\Omega = (\omega/\omega_0)$, $B = (\mu RL^3/mc^3 \omega_0)$, $\xi_2 = (c_1(l_1 + l_2)^2 + c_2l_2^2 + c_3l_3^2/J_d \omega_0^2)$, $\alpha_1 = (l_2[k_1(l_1 + l_2) + k_2l_2 - k_3l_3]/\omega_0^2 J_d)$, $F_r = (\mu RL^3/c^2) \bar{F}_r$, $F_{d1} = \zeta_1 \dot{Q}_1 + \zeta_2 \dot{Q}_2$, $\alpha_2 = (k_1(l_1 + l_2)^2 + k_2l_2^2 + k_3l_3^2/\omega_0^2 J_d)$, $F_1 = U \Omega^2 e^{i\Omega\tau} = (\delta/mc) (\omega^2/\omega_0^2) [\cos(\Omega\tau) + i \sin(\Omega\tau)]$, $F_{d2} = -\xi_1 \dot{Q}_1' - \xi_2 \dot{Q}_2'$, $F_t = (\mu RL^3/c^2) \bar{F}_t$, $F_r = (\mu RL^3/c^2) \bar{F}_r$, and $F_{c1} = -B \bar{F}_r (Q_1 + Q_2/e)$, $F_{c2} = -B \bar{F}_t (Q_1 + Q_2/e)$.

$$F_{c2} = -B \bar{F}_r \frac{Q_1 + Q_2}{e} - iB \bar{F}_t \frac{Q_1 + Q_2}{e}. \quad (22)$$

Because of $-i\Omega \eta \dot{Q}_2 = -\eta \ddot{Q}_2$, the corresponding homogeneous equation (21) is

$$\begin{cases} \ddot{Q}_1 + Q_1 + \kappa Q_2 = 0, \\ \ddot{Q}_2 + \frac{\alpha_1}{1-\eta} Q_1 + \frac{\alpha_2}{1-\eta} Q_2 = 0. \end{cases} \quad (23)$$

The corresponding characteristic equation is

$$\begin{aligned} \begin{vmatrix} 1-\lambda & \kappa \\ \alpha_1 & \alpha_2 - (1-\eta)\lambda \end{vmatrix} &= (1-\lambda)[\alpha_2 - (1-\eta)\lambda] - \kappa\alpha_1 \\ &= (1-\eta)\lambda^2 - \lambda(\alpha_2 + 1 - \eta) + \alpha_2 - \kappa\alpha_1 \\ &= 0. \end{aligned} \quad (24)$$

The natural frequency is

$$\lambda_1 = \omega_1^2$$

$$= \frac{\alpha_2 + 1 - \eta - \sqrt{(\alpha_2 + 1 - \eta)^2 - 4(1-\eta)(\alpha_2 - \kappa\alpha_1)}}{2(1-\eta)},$$

$$\lambda_2 = \omega_2^2$$

$$= \frac{\alpha_2 + 1 - \eta + \sqrt{(\alpha_2 + 1 - \eta)^2 - 4(1-\eta)(\alpha_2 - \kappa\alpha_1)}}{2(1-\eta)}. \quad (25)$$

The corresponding shape is

$$\begin{aligned} p_1 &= \frac{(1-\eta)\omega_1^2 - \alpha_2}{\alpha_1}, \\ p_2 &= \frac{(1-\eta)(1 - \omega_1^2)}{\alpha_1}. \end{aligned} \quad (26)$$

Therefore, the shape matrix is

$$P = \begin{pmatrix} p_1 & p_2 \\ 1 & 1 \end{pmatrix}. \quad (27)$$

Its inverse matrix is

$$\begin{aligned} P^{-1} &= \frac{1}{p_1 - p_2} \begin{pmatrix} 1 & -p_2 \\ -1 & p_1 \end{pmatrix} \\ &= \begin{pmatrix} \frac{1}{p_1 - p_2} & \frac{-p_2}{p_1 - p_2} \\ \frac{-1}{p_1 - p_2} & \frac{p_1}{p_1 - p_2} \end{pmatrix} \\ &= \begin{pmatrix} q_{11} & 1 - q_{22} \\ -q_{11} & q_{22} \end{pmatrix}, \end{aligned} \quad (28)$$

where $q_{11} = (1/p_1 - p_2)$, $q_{22} = (p_1/p_1 - p_2)$. Namely, $p_1 = (q_{22}/q_{11})$, $p_2 = (q_{22} - 1/q_{11})$.

Suppose that the influence of damping, the nonlinear factors, and the gyro effect are considered to be dimensionless. Assume that $\bar{Q} = P^{-1}Q$, $\omega_1 - \Omega = \varepsilon\sigma$. Further,

$$\begin{aligned}\bar{Q}_1'' + \omega_1^2 \bar{Q}_1 &= \varepsilon \frac{1}{p_1 - p_2} \left[U\Omega^2 e^{i\Omega\tau} - B\bar{F}_r \frac{(p_1+1)\bar{Q}_1 + (p_2+1)\bar{Q}_2}{e} - iB\bar{F}_t \frac{(p_1+1)\bar{Q}_1 + (p_2+1)\bar{Q}_2}{e} - \zeta_1(p_1\bar{Q}_1' + p_2\bar{Q}_2') - \zeta_2(\bar{Q}_1' + \bar{Q}_2') \right] \\ &+ \varepsilon \left(1 - \frac{p_1}{p_1 - p_2} \right) \left[-B'\bar{F}_r \frac{(p_1+1)\bar{Q}_1 + (p_2+1)\bar{Q}_2}{e} - iB'\bar{F}_t \frac{(p_1+1)\bar{Q}_1 + (p_2+1)\bar{Q}_2}{e} - \xi_1(p_1\bar{Q}_1' + p_2\bar{Q}_2') - \xi_2(\bar{Q}_1' + \bar{Q}_2') + i\Omega\eta(\bar{Q}_1' + \bar{Q}_2') \right] \\ \bar{Q}_2'' + \omega_2^2 \bar{Q}_2 &= -\frac{1}{p_1 - p_2} U\Omega^2 e^{i\Omega\tau} + \varepsilon \frac{1}{p_1 - p_2} \left[B\bar{F}_r \frac{(p_1+1)\bar{Q}_1 + (p_2+1)\bar{Q}_2}{e} + iB\bar{F}_t \frac{(p_1+1)\bar{Q}_1 + (p_2+1)\bar{Q}_2}{e} + \zeta_1(p_1\bar{Q}_1' + p_2\bar{Q}_2') + \zeta_2(\bar{Q}_1' + \bar{Q}_2') \right] \\ &+ \varepsilon \frac{p_1}{p_1 - p_2} \left[-B'\bar{F}_r \frac{(p_1+1)\bar{Q}_1 + (p_2+1)\bar{Q}_2}{e} - iB'\bar{F}_t \frac{(p_1+1)\bar{Q}_1 + (p_2+1)\bar{Q}_2}{e} - \xi_1(p_1\bar{Q}_1' + p_2\bar{Q}_2') - \xi_2(\bar{Q}_1' + \bar{Q}_2') + i\Omega\eta(\bar{Q}_1' + \bar{Q}_2') \right].\end{aligned}\quad (29)$$

The solution is obtained according to the resonance condition.

$$\begin{aligned}\bar{Q}_1 &= \bar{a}_1 e^{i(\Omega\tau + \theta_1)}, \\ \bar{Q}_1' &= i\omega_1 \bar{a}_1 e^{i(\Omega\tau + \theta_1)}, \\ \bar{Q}_2 &= \bar{a}_2 e^{i(\omega_2\tau + \theta_2)} - \frac{q_{11}U\Omega^2}{\omega_2^2 - \Omega^2} e^{i\Omega\tau}, \\ \bar{Q}_2' &= i\omega_2 \bar{a}_2 e^{i(\omega_2\tau + \theta_2)} - i \frac{q_{11}U\Omega^3}{\omega_2^2 - \Omega^2} e^{i\Omega\tau}.\end{aligned}\quad (30)$$

The average equation of the system can be obtained by the average method.

$$\begin{aligned}\frac{d\bar{a}_1}{d\tau} &= -\frac{\varepsilon}{2\omega_1} \frac{1}{p_1 - p_2} \left(U\Omega^2 \sin \theta_1 + B\bar{F}_t \frac{p_1+1}{e} \bar{a}_1 + \zeta_1 \omega_1 p_1 \bar{a}_1 + \zeta_2 \omega_1 \bar{a}_1 \right) \\ &+ \varepsilon \left(\frac{p_1}{p_1 - p_2} - 1 \right) \left[B'\bar{F}_t \frac{(p_1+1)\bar{a}_1}{e} + \omega_1 \xi_1 p_1 \bar{a}_1 + \omega_1 \xi_2 \bar{a}_1 \right],\end{aligned}\quad (31)$$

$$\frac{d\theta_1}{d\tau} = \omega_1 - \Omega - \frac{\varepsilon}{2\bar{a}_1 \omega_1} \frac{1}{p_1 - p_2} \left(U\Omega^2 \cos \theta_1 - B\bar{F}_r \frac{p_1+1}{e} \bar{a}_1 \right) - \frac{\varepsilon}{2\bar{a}_1 \omega_1} \left(\frac{p_1}{p_1 - p_2} - 1 \right) \left[\eta\Omega \bar{a}_1 \omega_1 + \frac{B'}{e} \bar{F}_r (p_1+1) \bar{a}_1 \right],\quad (32)$$

$$\frac{d\bar{a}_2}{d\tau} = -\frac{\varepsilon}{2\omega_2} \frac{1}{p_1 - p_2} \left[-\zeta_1 p_2 \bar{a}_2 \omega_2 - \zeta_2 \bar{a}_2 \omega_2 - \frac{B}{e} \bar{F}_t (p_2+1) \bar{a}_2 \right] + \frac{\varepsilon}{2\omega_2} \frac{p_1}{p_1 - p_2} \left[-\xi_1 p_2 \bar{a}_2 \omega_2 - \xi_2 \bar{a}_2 \omega_2 - \frac{B'}{e} \bar{F}_t (p_2+1) \bar{a}_2 \right],\quad (33)$$

$$\frac{d\theta_2}{d\tau} = -\frac{\varepsilon}{2\omega_2 \bar{a}_2} \frac{1}{p_1 - p_2} \frac{B}{e} \bar{F}_r (p_2+1) + \frac{\varepsilon}{2\omega_2 \bar{a}_2} \frac{p_1}{p_1 - p_2} \left[\eta\Omega \omega_2 + \frac{B'}{e} \bar{F}_r (p_2+1) \right].\quad (34)$$

It can be obtained from equation (33):

$$\left\{ \frac{1}{p_1 - p_2} \left[\zeta_1 p_2 \omega_2 + \zeta_2 \omega_2 + \frac{B}{e} \bar{F}_t (p_2 + 1) \right] - \frac{p_1}{p_1 - p_2} \left[\xi_1 p_2 \omega_2 + \xi_2 \omega_2 + \frac{B'}{e} \bar{F}_t (p_2 + 1) \right] \right\} \bar{a}_2 = 0. \quad (35)$$

Get

$$\begin{cases} \bar{a}_2 = 0, \\ \frac{1}{p_1 - p_2} \left[\zeta_1 p_2 \omega_2 + \zeta_2 \omega_2 + \frac{B}{e} \bar{F}_t (p_2 + 1) \right] - \frac{p_1}{p_1 - p_2} \left[\xi_1 p_2 \omega_2 + \xi_2 \omega_2 + \frac{B'}{e} \bar{F}_t (p_2 + 1) \right] = 0. \end{cases} \quad (36)$$

Therefore,

$$\begin{cases} \frac{1}{p_1 - p_2} (\zeta_1 p_2 + \zeta_2) - \frac{p_1}{p_1 - p_2} (\xi_1 p_2 + \xi_2) < 0, \\ \frac{1}{p_1 - p_2} B - \frac{p_1}{p_1 - p_2} B' < 0. \end{cases} \quad (37)$$

According to equation (37) and literature [23], it can be seen that $\|\bar{Q}_2\| \ll \|\bar{Q}_1\|$.

Since $Q_1 = p_1 \bar{Q}_1 + \varepsilon p_2 \bar{Q}_2$ and $Q_2 = \bar{Q}_1 + \varepsilon \bar{Q}_2$, $a_1 = \|Q_1\| \approx p_1 \bar{a}_1$ and $a_2 = \|Q_2\| \approx \bar{a}_1$ are get.

Choosing the dimensionless of $\Omega_1 = \Omega/\omega_1$, we can combine it with equations (32) and (33):

$$\begin{aligned} & \left[(2\omega_1 p_2 B' - B) \bar{F}_t \frac{(p_1 + 1)a_1}{p_1 e} + (2\omega_1^2 p_2 \xi_1 - \zeta_1 \omega_1) a_1 + (2\omega_1^2 p_2 \xi_2 - \zeta_2 \omega_1) \frac{a_1}{p_1} \right]^2 \\ & + \left[2 \frac{a_1}{p_1} \omega_1^2 (p_1 - p_2) (1 - \Omega_1) - p_2 \eta \Omega_1 \frac{a_1}{p_1} \omega_1^2 + (B - p_2 B') \bar{F}_r \frac{p_1 + 1}{e} \frac{a_1}{p_1} \right]^2 = (U \Omega_1^2 \omega_1^2)^2. \end{aligned} \quad (38)$$

Hence, considering $(e/c) = (p_1 + 1/p_1)a_1$, the bifurcation equation is obtained:

$$\begin{aligned} G = & \left[(2\omega_1 p_2 B' - B) \bar{F}_t^* + (2\omega_1^2 p_2 \xi_1 - \zeta_1 \omega_1) a_1 + (2\omega_1^2 p_2 \xi_2 - \zeta_2 \omega_1) \frac{a_1}{p_1} \right]^2 \\ & + \left[2 \frac{a_1}{p_1} \omega_1^2 (p_1 - p_2) (1 - \Omega_1) - p_2 \eta \Omega_1 \frac{a_1}{p_1} \omega_1^2 + (B - p_2 B') \bar{F}_r^* \right]^2 - (U \Omega_1^2 \omega_1^2)^2. \end{aligned} \quad (39)$$

Then, equivalent oil film forces of \bar{F}_r and \bar{F}_t are

$$\begin{aligned} \bar{F}_r^* &= \frac{2p_1^2 (p_1 + 1)^2 a_1^2}{[p_1^2 - (p_1 + 1)^2 a_1^2]^2} - \frac{2\pi v_d p_1^4 (p_1 + 1) a_1}{c [p_1^2 - (p_1 + 1)^2 a_1^2]^{5/2}}, \\ \bar{F}_t^* &= \frac{\pi p_1^2 (p_1 + 1) a_1}{2 [p_1^2 - (p_1 + 1)^2 a_1^2]^{3/2}} - \frac{2v_d p_1^2}{c [p_1^2 - (p_1 + 1)^2 a_1^2]}. \end{aligned} \quad (40)$$

Singularity theory analyzes the bifurcation set, lag set, and transition set [23]. In this study, these can be also obtained using the bifurcation formula (39). However, in the analysis process, the interesting factors cannot be analyzed. For example, the coefficient of bearing in the literature includes the viscosity coefficient of the oil film, quality of the

bearing, oil clearance, and precession speed. Therefore, they are unable to describe the influence of various parameters on some specific structures. In this study, according to the basic theory and thought of the singularity theory, a numerical simulation is used to discuss the relevant structural parameters to verify relevant theories.

4. Numerical Simulation

Based on the above theoretical analysis, the relevant simulation parameters for the ERSFD rotor system are selected, as shown in Table 1. Different amplitude modes obtained concerning the bearing coefficient and parameters of the rotor eccentricity, hole of oil seepage, and stiffness and

TABLE 1: Parameters of the ERSFD rotor system.

Physical description	Parameter	Value
Equivalent mass of the rotor	m (kg)	643
Equivalent equatorial moment of inertia	J_d ($\text{kg}\cdot\text{m}^2$)	15
Equivalent polar moment of inertia	J_p ($\text{kg}\cdot\text{m}^2$)	30
Distance from elastic support 1 to elastic support 2	l_1 (m)	0.28
Distance from elastic support 2 to disk center	l_2 (m)	1.28
Distance from disk center to elastic support 3	l_3 (m)	0.62
Stiffness coefficient of elastic support 1	k_1 (N/m)	1.0×10^6
Stiffness coefficient of elastic support 2	k_2 (N/m)	3.0×10^6
Stiffness coefficient of elastic support 3	k_3 (N/m)	6.0×10^6
Rotor unbalance value	δ ($\text{kg}\cdot\text{m}$)	3.5×10^{-3}
Clearance of squeeze film damper	c (m)	3.0×10^{-4}
Radius of the journal	R (m)	265×10^{-3}
Length of squeeze film damper	L (m)	15×10^{-3}
Height of boss	h_{00} (m)	0.5×10^{-4}
Thickness of elastic ring	h_{01} (m)	3.5×10^{-4}
Kinetic viscosity coefficient of oil film	μ (N·s/m)	6.76×10^{-3}

position of elastic supports are analyzed to improve the range optimization of parameters.

Figure 4 describes the theoretical analysis results of SFD and SREFD under the proposed method in this paper and the numerical calculation results by using the fourth-order Runge–Kutta method. The numerical results calculated are consistent with theoretical analysis results in this paper, which verifies the feasibility of the method in this study. By analyzing the intersection of SFD and ERSFD kinds of structure, it can be seen that the amplitude of the SFD rotor system at point A is significantly higher than the amplitude of the ERSFD rotor system. The oil film force plays a significant role in the low precession speed of the shaft. When the rotor speed increases due to the precession speed rising, vibration suppression of the elastic ring increases, which is consistent with the overall effect. The impact of the ERSFD on vibration suppression is better than that of SFD, and the maximum amplitude of ERSFD at the peak is reduced by 10% compared with that of SFD.

By considering the nondimensional integrated unbalance value U (the oil clearance, unbalance value, and rotor mass), the nondimensional damper-bearing parameter B (the rotor mass, oil film viscosity coefficient, oil clearance, length and radius of the shaft, and precession speed), and the flow permeability of the oil film of the elastic ring, the vibration conditions of the ERSFD rotor system are discussed and analyzed in Figures 5(a)–5(e).

As shown in Figure 5(a), the maximum amplitude gradually decreased with increasing B . There are two different kinds of amplitudes in the speed range of $[0, 0.9]$ during $B \in (0.04, 0.08)$. At $B = 0.0963$, the amplitude increased. In Figure 5(b), the maximum amplitude increases with an increase in U . At $U = 6e - 4$ and $U = 2e - 4$, the effect of the unbalanced value on the amplitude can be ignored when Ω_1 exceeds 1. Refer to some relevant papers; there are different bifurcation forms consistent with the trend analyzed by the bifurcation set and the transition set [23].

To further analyze the influence of related parameters, Figures 5(c) and 5(d) study the unbalance value δ and some parameters of the ERSFD in detail. As shown in Figure 5(c),

the amplitude gradually increases with an increase in the unbalance, and the overall trend does not change. However, the speed of the maximum amplitude increases gradually.

In Figure 5(d), the relationship between the rotor speed and amplitude of the process of the elastic ring moving from the suspension to the inner and outer bosses contact is analyzed theoretically. The essence of the moving process of the elastic ring from the suspension to the inner and outer bosses contact is to change the oil film clearance through extrusion and produce different oil film forces. Therefore, according to the structural parameters, different values of c were selected to describe the process. Assuming that the height of the inner and outer bosses is $h_{00} = 0.5e - 4$ m, the curve of $c = 3.5e - 4$ m and the curve of $c = 3.0e - 4$ m describe the position between two bosses and the oil film force effect of the boss position, respectively. Of course, this can also describe the amplitude frequency curve of the oil film clearance change from the perspective of elastic ring movement. With smaller oil film clearance, the amplitude gradually decreases. Mainly the oil film force increases, which suppresses vibration. When the clearance is less than the height of the boss, its primary role is that the supporting force of the elastic ring is greater than that of the oil film force between the two bosses. Furthermore, as shown in Figure 5(e), with the increased flow permeability of the oil film of the elastic ring, the amplitude decreases gradually at the same speed. This implies that the oil film has a significant dampening effect. Otherwise, the size of the oil hole's permeability is affected by the structural parameters of the elastic ring, which provides the theoretical basis for the analysis and design of the structural parameters of the elastic ring.

The vibration influence of the stiffness and distance of the supporting system is shown in Figures 6(a) and 6(b). As shown in Figure 6(a), when $k_2 = 2e7$ N/m and $k_3 = 8e7$ N/m, there are more complex vibration forms. When $k_2 = 3e7$ N/m and $k_3 = 7e7$ N/m, the amplitudes are the smallest. The order of amplitude corresponding to each stiffness value is different in the speed interval of less than 0.8 and higher than 1.1. Overall, the initial parameters (as shown in A) selected in this study are reasonable. As the support stiffness increases,

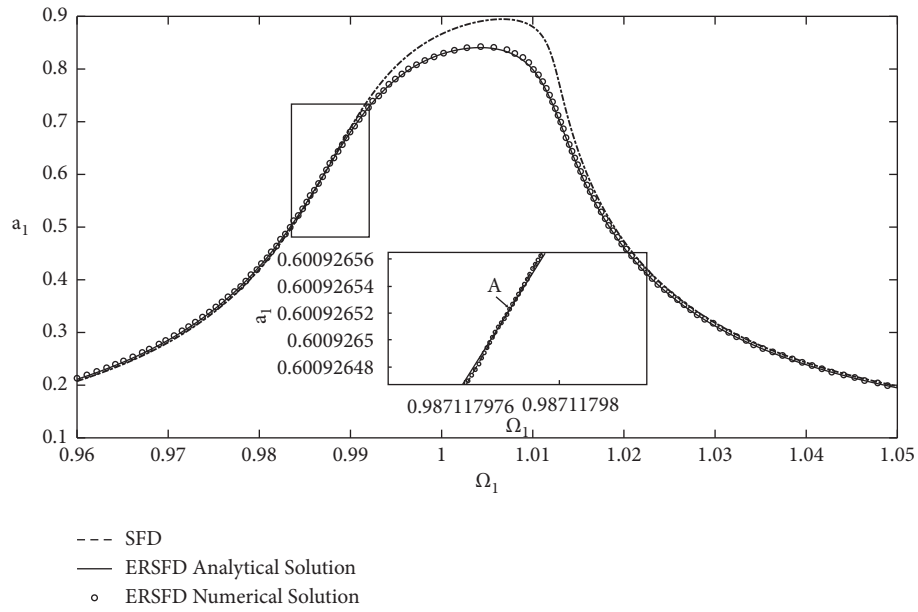


FIGURE 4: Amplitude frequency curves.

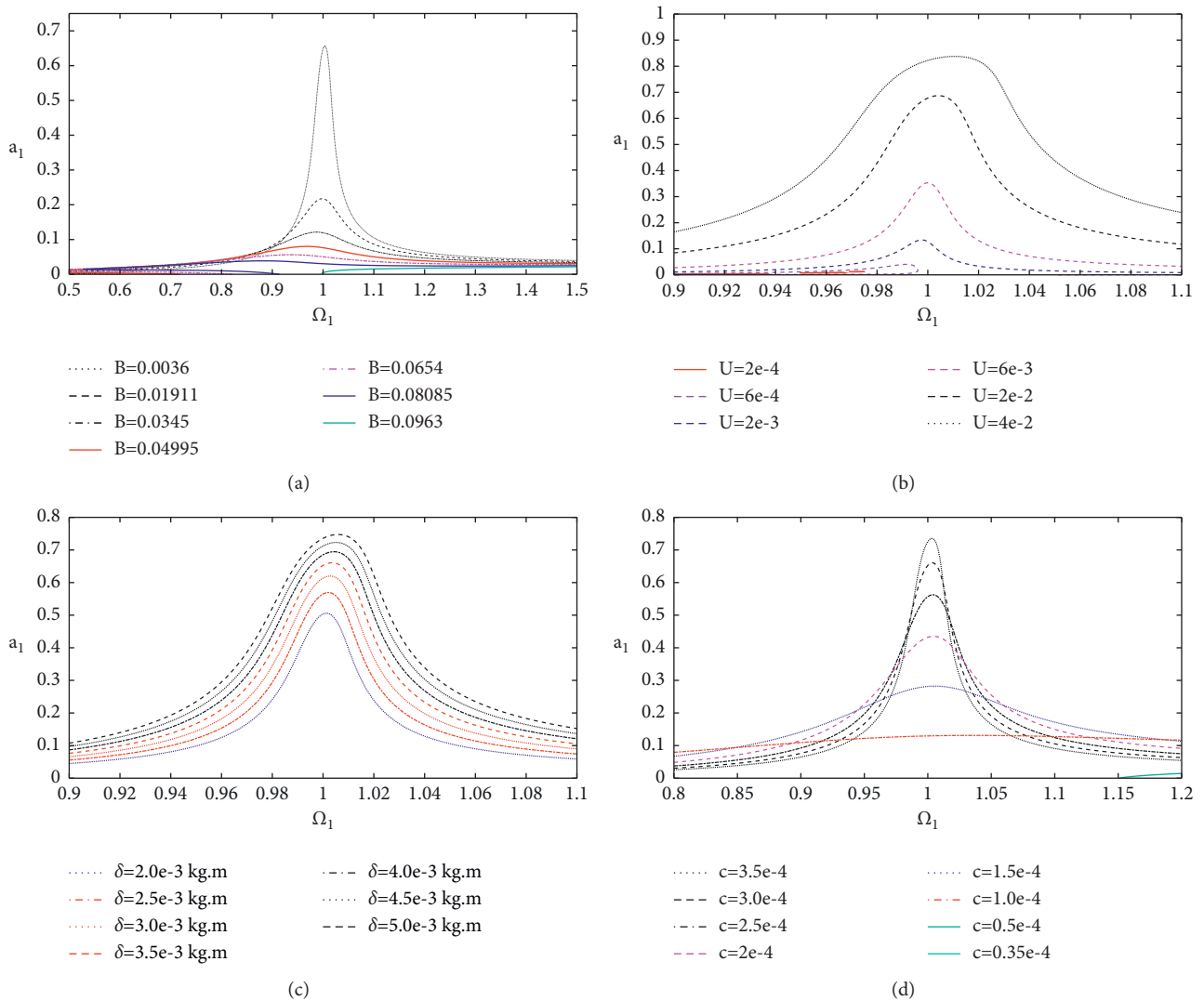


FIGURE 5: Continued.

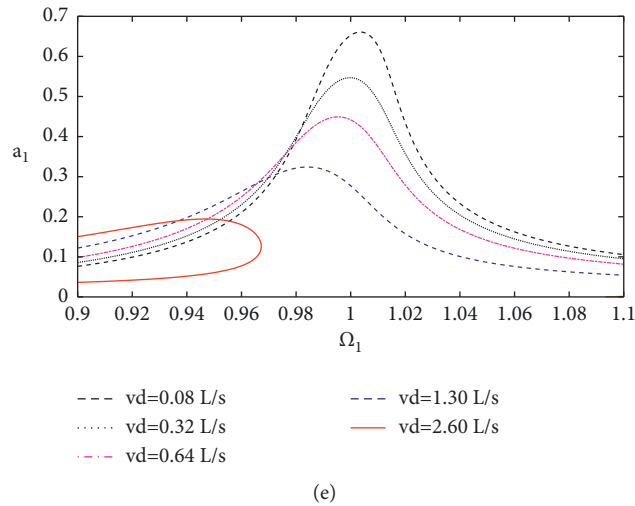


FIGURE 5: (a) Amplitude frequency curves of $B, U = 0.018$. (b) Amplitude frequency curves of $U, B = 0.0036$. (c) Amplitude frequency curves of $\delta, c = 3.0e - 4$ m. (d) Amplitude frequency curves of the process of elastic ring moving from the suspension to the inner and outer contact, $\delta = 3.5e - 3$ kg-m. (e) Amplitude frequency curves of the permeability oil hole, $c = 3.0e - 4, \delta = 3.5e - 3$ kg-m.

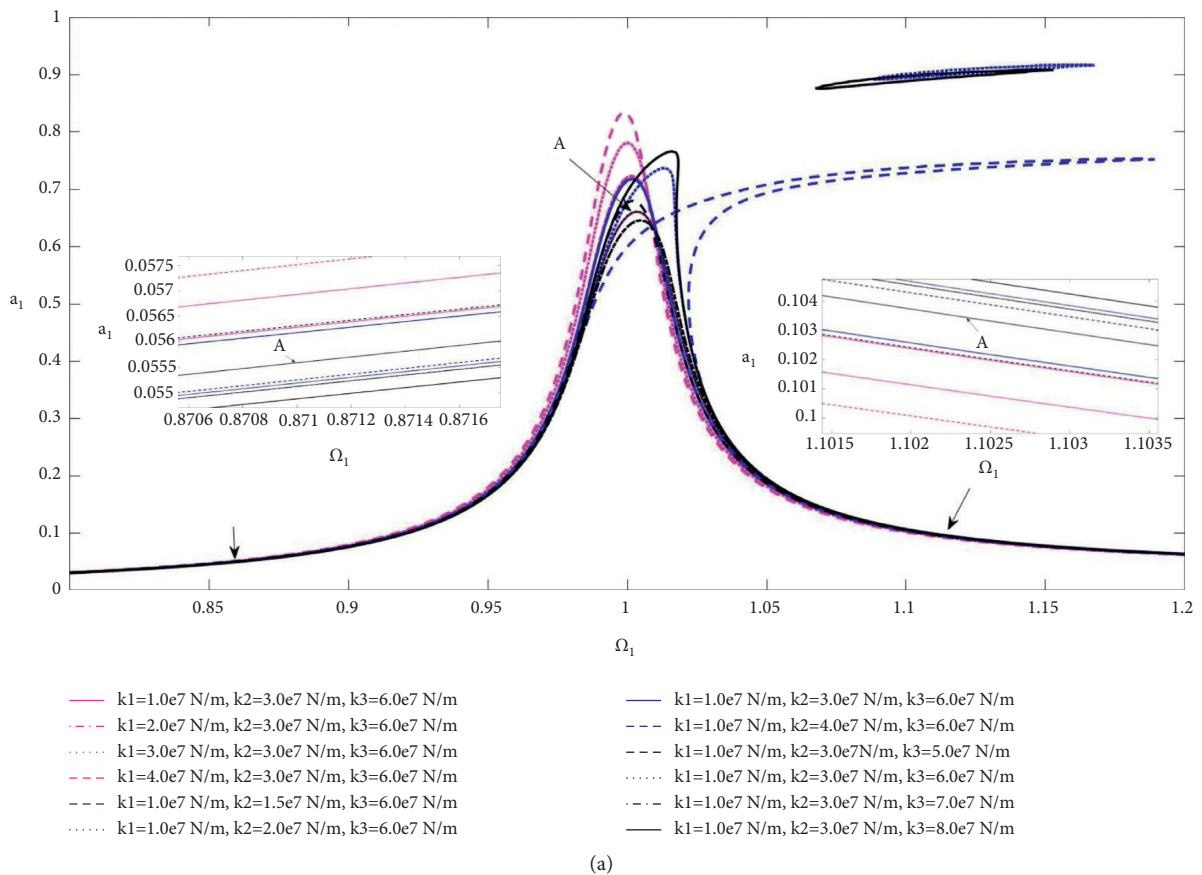


FIGURE 6: Continued.

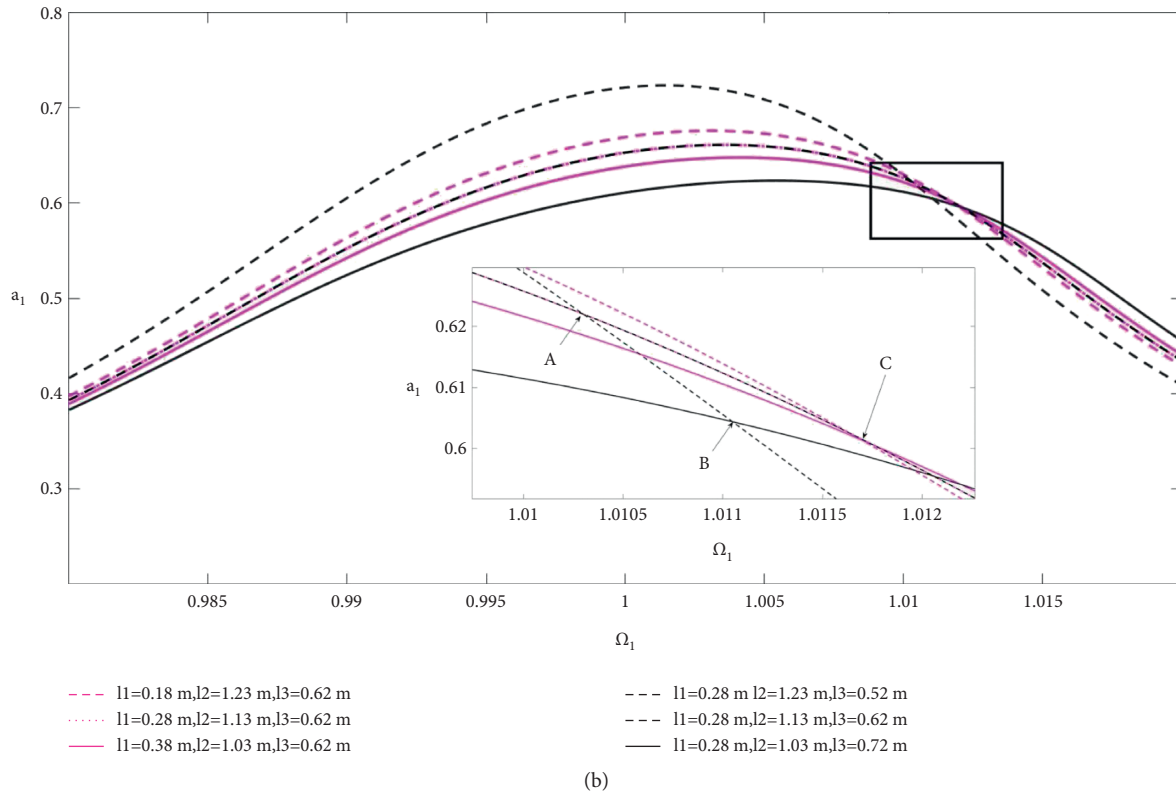


FIGURE 6: (a) Amplitude frequency curves of the bearing stiffness. (b) Amplitude frequency curves of the bearing positions l_1 , l_2 , and l_3 .

the amplitude of the support changes slightly, resulting in different bifurcation structures [23]. This is consistent with the results of previous studies.

As shown in Figure 6(b), the amplitude effect at different distances is significant. The total length of the rotor shaft remains unchanged, and the positions of elastic supports 1 and 3 at both ends are changed. As can be seen, the maximum amplitude decreases gradually as the distance increases at the resonance point. However, as the rotor speed increases, at point C, the amplitude gradually increases with a decrease in l_1 . At points A and B, as the value of l_3 decreases, the amplitude gradually increases. Therefore, the elastic modulus and installation position should be considered comprehensively in actual operation.

Based on the above discussion, the unbalanced value of the dimensional, bearing parameter, permeability flow rate of the oil hole, support stiffness, and supporting position are all discussed with the vibration analysis. It can be seen that, in comparison to SFD, ERSFD effectively suppressed the amplitude, and the influence of structural parameters had different amplitude frequency curves, including the process of elastic ring moving from the suspension to the inner and outer bosses contact, permeability oil hole, bearing stiffness, and bearing position.

5. Conclusion

In this study, a model of the elastic ring squeeze film damper, elastic support, and rotor system dynamics were estimated. The short bearing theory approximates the analytical

solution of the inner oil film forces of the suspension and the inner and outer bosses contact. Considering the oil film stiffness and damping of rolling bearings, the elastohydrodynamic lubrication (EHL) model is used to describe the supports stiffness of the rolling bearing. The average approach is used to analyze the relationships between system parameters. The specific conclusions are as follows:

- (1) The dynamic characteristics of the ERSFD rotor system can be significantly improved over the SFD rotor system, and the vibration amplitude can be decreased.
- (2) With an increase in the nondimensional damper-bearing parameter, the maximum amplitude gradually decreases. However, the maximum amplitude increases with an increase in the nondimensional integrated unbalanced value.
- (3) As the unbalanced value increases, the amplitude gradually increases, and the overall trend does not change. Nevertheless, the speed of the maximum amplitude increases gradually.
- (4) According to the structural parameters, different values of c are selected to describe the process of the elastic ring from the suspension to the inner and outer bosses contact. With a minor oil film clearance, the oil film force increases, and the amplitude gradually decreases. The flow permeability of the oil film of the elastic ring increases, and the amplitude

decreases gradually. This implies that the oil film has a significant dampening effect.

- (5) The amplitude changes as the stiffness changes. At the resonance point, the maximum amplitude gradually decreases with an increase in the distance. The elastic modulus and the installation position should be comprehensively considered in the actual operation.

Different regions have different amplitudes of parameter values. These results will contribute to the decision-making process for unsymmetrical rotor system simplification and understanding the nonlinear dynamic behaviors of ERSFD rotor systems for parameter optimization.

Data Availability

The data used to support the findings of this study are included within the article.

Conflicts of Interest

The authors declare that they have no conflicts of interest.

Acknowledgments

This work was supported by the National Science and Technology Major Project (no. 2017-IV-0008-0045) and the National Natural Science Foundation of China (no. 11872045).

References

- [1] C. S. Zhu and X. H. Feng, "An experimental investigation on the bistable behaviors of a flexible rotor squeeze film damper system," *Journal of Aerospace Power*, vol. 2, no. 3, pp. 105–108, 1988.
- [2] G. Meng and N. Xia, "Bifurcation and chaos responses of a flexible rotor-squeeze film damper system," *Acta Aeronautica et Astronautica Sinica*, vol. 1, no. 24, pp. 42–45, 2003.
- [3] N. Xia, G. Meng, and Y. B. Fan, "The optimum parameters selection of a over-hung flexible rotor with two disks supported on centralized squeeze film damper," *Chinese Journal of Applied Mechanics*, vol. 2, no. 17, pp. 51–55, 2000.
- [4] M. A. Rezvani and E. J. Hahn, "Floating ring squeeze film damper: theoretical analysis," *Tribology International*, vol. 3, no. 33, pp. 249–258, 2000.
- [5] J. Y. Zhao, I. W. Linnett, and L. J. McLean, "Stability and bifurcation of unbalanced response of a squeeze film damped flexible rotor," *Journal of Tribology*, vol. 2, no. 116, pp. 361–368, 1994.
- [6] Z. L. Wang, N. Xu, X. Y. Yu, and G. H. Zhang, "The dynamic characteristic analysis of elastic ring squeeze film damper by fluid-structure interaction approach," in *Proceedings of the ASME Turbo Expo 2017: Turbomachinery Technical Conference and Exposition*, Charlotte, NC USA, June 2017.
- [7] Z. Han, Q. Ding, and W. Zhang, "Dynamical analysis of an elastic ring squeeze film damper-rotor system," *Mechanism and Machine Theory*, vol. 131, pp. 406–419, 2019.
- [8] Z. L. Wang, G. H. Zhang, J. Q. Wen, and Z. S. Liu, "Numerical modeling of the flow in the squeeze film dampers with oil feed groove by computational fluid dynamic analysis," *Participant Journal: Journal of Engineering Tribology*, vol. 231, no. 6, pp. 693–707, 2017.
- [9] Y. Li, M. F. Liao, and S. J. Wang, "Effect on vibrating attenuation by the fit of elastic ring squeeze film damper," *Journal of Vibration and Shock*, vol. 39, no. 11, pp. 232–238, 2020.
- [10] Y. Xu, X. Chen, J. Zou, W. Qi, and Y. Li, "Influence of orifice distribution on the characteristics of elastic ring squeeze film dampers for flywheel energy storage system," *IEEE Transactions on Plasma Science*, vol. 5, no. 14, pp. 1272–1279, 2013.
- [11] M. Zhou, Q. H. Li, and H. T. Yan, "Mechanism study of the Porous ring squeeze film dampers (1)," *Gas Turbine Experiment and Research*, vol. 4, no. 11, pp. 19–31, 1998.
- [12] H.-l. Zhou, G.-h. Luo, G. Chen, and F. Wang, "Analysis of the nonlinear dynamic response of a rotor supported on ball bearings with floating-ring squeeze film dampers," *Mechanism and Machine Theory*, vol. 59, pp. 65–77, 2013.
- [13] M. Zhou, Q. H. Li, and H. T. Yan, "Application of Flexible-Porous squeeze film damped support to a core engine," *Journal of Aerospace Power*, vol. 4, no. 13, pp. 403–407, 1998.
- [14] J. Li, S. Q. Cao, H. L. Guo, R. M. Nie, and Y. H. Hou, "Vibration performance of dual rotor systems considering elastohydrodynamic lubrication of intershaft bearings," *Journal of Harbin Institute of Technology*, vol. 53, no. 6, pp. 138–147, 2021.
- [15] M. Tiwari, K. Gupta, and O. Prakash, "Dynamic response of an unbalanced rotor supported on ball bearings," *Journal of Sound and Vibration*, vol. 5, no. 238, pp. 757–779, 2000.
- [16] S. H. Gao, X. H. Long, and G. Meng, "Nonlinear response and nonsmooth bifurcations of unbalanced machine-tool spindle-bearing system," *Nonlinear Dynamics*, vol. 4, no. 54, pp. 365–377, 2008.
- [17] T. A. Harris, *Rolling Bearing Analysis*, John Wiley & Sons, New York, NY, USA, 3rd edition, 1990.
- [18] J. Liu, "A dynamic modelling method of a rotor-roller bearing-housing system with a localized fault including the additional excitation zone," *Journal of Sound and Vibration*, vol. 469, no. 3, pp. 1–18, 2020.
- [19] K. K. Shi, S. J. Zhang, L. X. Li, M. J. Wang, and T. L. Zhang, "Research on detection method for radial stiffness of elastically supported bearing rings," *Bearing*, vol. 4, no. 4, pp. 63–66, 2019.
- [20] G. Q. Feng and B. Z. Zhou, "Optimization design and test investigation of squirrel cage elastic support," *Journal of Aerospace Power*, vol. 1, no. 26, pp. 199–203, 2011.
- [21] R. Tang, J. Guo, Z. Luo, D. Y. Wang, and Y. Q. Liu, "Optimal Design method of squirrel cage elastic support by stages," *Aeroengine*, vol. 42, no. 2, pp. 38–43, 2016.
- [22] G. Q. Feng, B. Z. Zhou, and J. Wang, "Fatigue strength analysis of squirrel cage elastic support based on global-local technology," *Aeroengine*, vol. 3, no. 33, pp. 22–24, 2007.
- [23] H. Z. Chen, L. Hou, and Y. S. Chen, "Bifurcation analysis of a rigid-rotor squeeze film damper system with unsymmetrical stiffness supports," *Archive of Applied Mechanics*, vol. 87, no. 4, pp. 1347–1364, 2017.